EFFECT OF TWO-STEP SOLUTION TREATMENTS ON THE MICROSTRUCTURE AND MECHANICAL PROPERTIES OF B357 ALUMINUM ALLOY

Neset Akar, Omer Sahin and Volkan Kilicli
Department of Metallurgical and Materials Engineering, Faculty of Technology, Gazi University, 06560 Teknikokullar, Ankara, Turkey

https://doi.org/10.1007/s40962-024-01320-w

Abstract

This study investigates the effect of two-step solution treatments and aging times on the microstructure and mechanical properties of B357 Al–Si alloy, part of the most widely used cast aluminum alloy. Three sets of artificial aging heat treatments were conducted on the tensile samples prepared from B357 alloy produced by low-pressure die casting. Firstly, the conventional artificial aging heat treatment (T6) was carried out by solutionizing the tensile samples at 543 °C for 8.5 h, water quenching at 60 °C, and then artificially aging for 8.5 h at 160 °C. In the two-step solution treatment, the samples were solutionized at 400, 440, 480, and 520 °C for 4 h and then solutionized at 543 °C for 8.5 h and water quenched to 60 °C and then artificially aged for 8.5 h at 160 °C. Thirdly, the samples were solutionized at 480 °C for 4 h, solutionized at 543 °C for 8.5 h, water quenched to 60 °C, and artificially aged for 3–192 h. Despite different solutioning and aging processes, no significant differences were observed in the microstructures of the samples. Si particle coarsening was observed with increasing solution temperature (400–520 °C) and aging times (3–192 h). Si-containing dispersoids and dispersoid-free zones (DFZ) were observed in the primary-α matrix. While DFZ width increased with temperature and aging, dispersoid zones in primary-α dendrites significantly decreased. Differential Scanning Calorimetry (DSC) analysis shows that two-step solution treatment in B357 alloy increases β′ precipitates for Mg_2Si precipitation strengthening. The two-step solutionized and aged sample showed the best combination of strength and ductility among all aged samples. B357 alloy exhibited the highest yield and tensile strength (309.7, 366.1 MPa) with 6% elongation for two-step solutionizing and 48 h aging. All aged B357 alloys showed ductile fracture as the primary fracture mode. However, brittle fractured Si particles were observed on the fracture surfaces.

Keywords: *B357 alloy, two-step solution treatment, aging times, microstructure, mechanical properties, 357 aluminum*

Introduction

Hypoeutectic cast Al–Si alloy is the most widely used cast aluminum alloy in industrial applications due to its exceptional castability, higher mechanical properties, and lower cost.[1] In recent years, the demand for cast Al–Si alloys has remarkably increased in the automotive industry, particularly in electric cars, due to their strength-to-weight ratio.[1,2]

The mechanical properties of Al–Si cast alloys strongly depend on the Mg level selected, the aging heat treatments, and microstructural features. Artificial aging heat treatment (T6) increases the yield and ultimate tensile strength of Al–Si casting alloys with good ductility by more than 1.5 times.[3–7] Besides, the solution in the aging process refines and homogenizes the microstructures of Al–Si cast alloys, particularly its spheroidized the eutectic Si particles.[8–11] Solution temperatures and times significantly affect cast Al–Si alloys' microstructures and mechanical properties.[9,10,12–15] Researchers have tried to improve the mechanical properties of cast Al–Si alloys by controlling the temperature and times for solution and aging treatments.[8–10,16–18] Several studies have been conducted on optimizing aging times and temperatures of cast Al–Si alloys for improved mechanical properties.[9,10,12,19,20] In addition, the effect of solution temperature on

Received: 08 January 2024 / Accepted: 13 March 2024
Published online: 24 April 2024

microstructures and mechanical properties has been studied by several authors.[8–10,14,15,18,21,22] Solution treatments at a higher temperature are an effective way to reduce the treatment times. However, if not carefully controlled it may lead to grain boundary incipient melting[11] and coarsening of the eutectic Si particles.[10] Moreover, the solution treatments at a higher temperature are not cost-effective.[8,9,18]

The authors mostly performed a single-step solution treatment in the artificial aging (T6) process.[12,18,20,21,23–27] The T6 aging process is time-consuming, and optimized heat treatment parameters can significantly improve manufacturing efficiency and cost-effectiveness. Toschi[27] reported that two-step solution treatment significantly enhanced the mechanical properties of A354 alloy with lower processing times. Improved hardness and tensile strength, along with good ductility, were achieved. Samuel et al.[28] reported that ductility was improved in A319.2 alloy by two-step solution treatment. Han et al.[9] indicated that a two-step solution treatment obtained the best combination of the mechanical properties for 319 alloys. Moreover, the two-step solution treatment provides more solute elements in the matrix and increases the degree of super-saturated solid solution (SSSS).[9,27]

So far, no study has been found investigating the effects of two-step solution processes and aging times on the microstructure and mechanical properties of B357 Alloy. In this study, the effect of two-step solution treatment with different first-step solution treatment temperatures (400–520 °C) and different aging times (3–192 h) on the microstructures and mechanical properties of B357 was investigated.

Experimental Procedures

Materials and Casting Process

After 750 kg of B357 alloy ingot with low iron content was melted in a graphite crucible using an electric resistance furnace, its chemical composition was analyzed to ensure the iron content. AlTi5B1 rod was added 22.5 kg into the melt to grain refinement, obtaining 0.15 wt.- %Ti content. AlSr15 rod was added 1.25 kg into the melt to Si modifier, obtaining 0.25 wt.%Sr content. The degassing process was carried out in a fully automatic degassing machine at 450 rpm under Argon gas for 10 minutes using Sheffer Arsal granule flax. The gas density index of liquid metal was checked and confirmed to be in the range of 0–1. After all casting processes, the chemical composition was analyzed using a Spectromaxx optical emission spectrometer (OES). The chemical composition of the B357 alloy used in this study is given in Table 1. Tensile test bars were manufactured by a low-pressure die casting method (Figure 1a). Liquid metal at 750 °C was filled into a steel mold preheated to 400 °C at a pressure of 320 mbar. The tensile bar mold was designed with SOLIDCAST casting simulation software and guaranteed free of casting defects such as micro or macro shrinkage. All cast tensile bars were examined using Zeiss Bosello Max70/120 X-ray radiography (Figure 1b). Grade B as the level of X-ray radiography according to AMS-A-21180 standard was determined in tensile samples.

Heat Treatments

An electrical resistance laboratory furnace with a temperature accuracy of ±1° C was used for solution treatments and aging. The temperature of tensile bar samples was monitored with a time-temperature recorder. The furnace is not equipped with air circulation. The heating rate and solution times are recorded in an Excel file. The heating rate is 0.6 °C/s. Quenching delay from solution temperature was kept lower than 5 s. The water bath has no water circulation. The delay between quenching and starting the aging is less than one hour.

In conventional aging treatment (T6), solution and aging temperatures were selected as 543 and 160 °C, respectively, according to the AMS 2771E standard.[29] Tensile samples were solutionized at 543 °C for 8.5h and then water-quenched into the 60 °C bath. The bars were aged at 160 °C for 9 h and cooled in air. In the two-step solution treatment, first-step solution temperatures were selected as 400, 440, 480, and 520 °C for 4 h, and the second-step

Table 1. Chemical Compositions (wt.%) of B357 Alloy

Alloy	Si	Mg	Fe	Cu	Mn	Ti	Zn	B	V	Sr	Na	Al
B357.0	6.5–7.5	0.4–0.6	Max 0.09	Max 0.05	Max 0.05	0.04–0.2	Max. 0.05	Total max. 0.15				Remain
OES analysis result	7.29	0.57	0.086	0.018	0.006	0.154	0.004	0.008	0.011	0.025	0.002	Remain

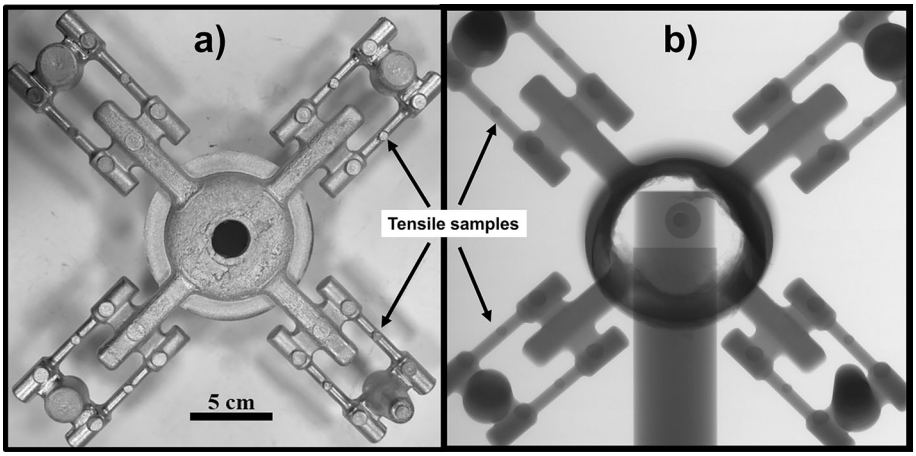

Figure 1. B357 alloy tensile bars: (a) parts produced by low-pressure die casting, and (b) X-ray radiography images of the part.

solution was kept constant at 543 °C for 8.5 h. The samples were water-quenched into the 60 °C bath. The bars were aged again at 160 °C for 9 h and cooled in air. The best mechanical properties were obtained at 480 °C, the first-step solution temperature mentioned in Section "Mechanical Properties". The samples were aged for 3 h–192 h at 160 °C following two-step solutionized at 480 °C for 4 h and 543 °C for 8.5 h to investigate the effect of aging times on the mechanical properties. A summary of the heat treatments is shown schematically in Figure 2.

Materials Characterization

Metallographic samples were cut from the undeformed region of the tensile bars and cold-mounted for grinding and polishing with colloidal silica suspension down to 0.1 μm and finally etched with 0.5% HF reagent. Leica DMI 5000M inverted optical microscope, Hitachi SU5000 scanning electron microscope (SEM), and Oxford Instruments X-MaxN 80 model energy-dispersive X-ray spectrum analysis (EDX) were used to characterize the microstructures and fracture surfaces. The volume fraction and particle size of Si particles were measured by using Leica Application Suite image analysis software version 4.6. A minimum of 9 mm^2 square was scanned on each heat treatment condition to characterize eutectic Si particles quantitatively. X-ray diffraction patterns were obtained on a Bruker D8 Advance X-ray diffractometer and operated at 40 kV and 40 mA using monochromatic Copper Kα radiation (λ = 1.5406 A°). Samples were scanned in the 2θ range of 30–90° at a scanning speed of 0.05°/min. Thermal analysis was performed using the Hitachi DSC7020 model for differential scanning calorimetry (DSC) to identify precipitation reactions after aging treatments. DSC experiments were performed in an argon atmosphere, and the samples were heated from 100 to 350 °C at a heating rate of 10 °C/min. Tests were conducted using samples weighing 1.8 mg each in aluminum pans.

Mechanical Tests

Tensile and hardness tests were performed to determine the mechanical properties of the samples. Tensile tests were conducted using an Instron 3369 universal testing machine at a strain rate of 0.00025 s^{-1}. The tensile bar is illustrated in Figure 3. A clip-on extensometer was used to measure the gauge length strain at 25 mm. Five tensile samples were tested for each heat treatment condition, and the average values were taken. Hardness tests were performed with the Brinell hardness test method (2.5 mm WC ball and 31.25 kgf) on the Emcotest DuraVision 200 hardness tester. At least five different indentations were taken, and their mean values were presented.

Results and Discussion

Microstructural Examinations

The optical microstructures of the B357 alloy are shown in Figures 4 and 5, respectively, based on the first-step solution temperatures and aging times. The as-cast microstructure of B357 alloy consisted mainly of primary-α dendrites with the mean secondary dendrite arm spacing (SDAS) of 25 μm and eutectic silicon structure (Figure 4a). The eutectic silicon structures are uniformly distributed around primary-α dendrites without casting defects, as shown in Figure 4.a. It was observed that very fine eutectic structures were formed in small fibrous shapes due to Sr modification.

Figures 4 and 5 show that different aging treatment conditions lead to similar microstructures, with minor variations attributed to the coarsening of Si particles. It is well-

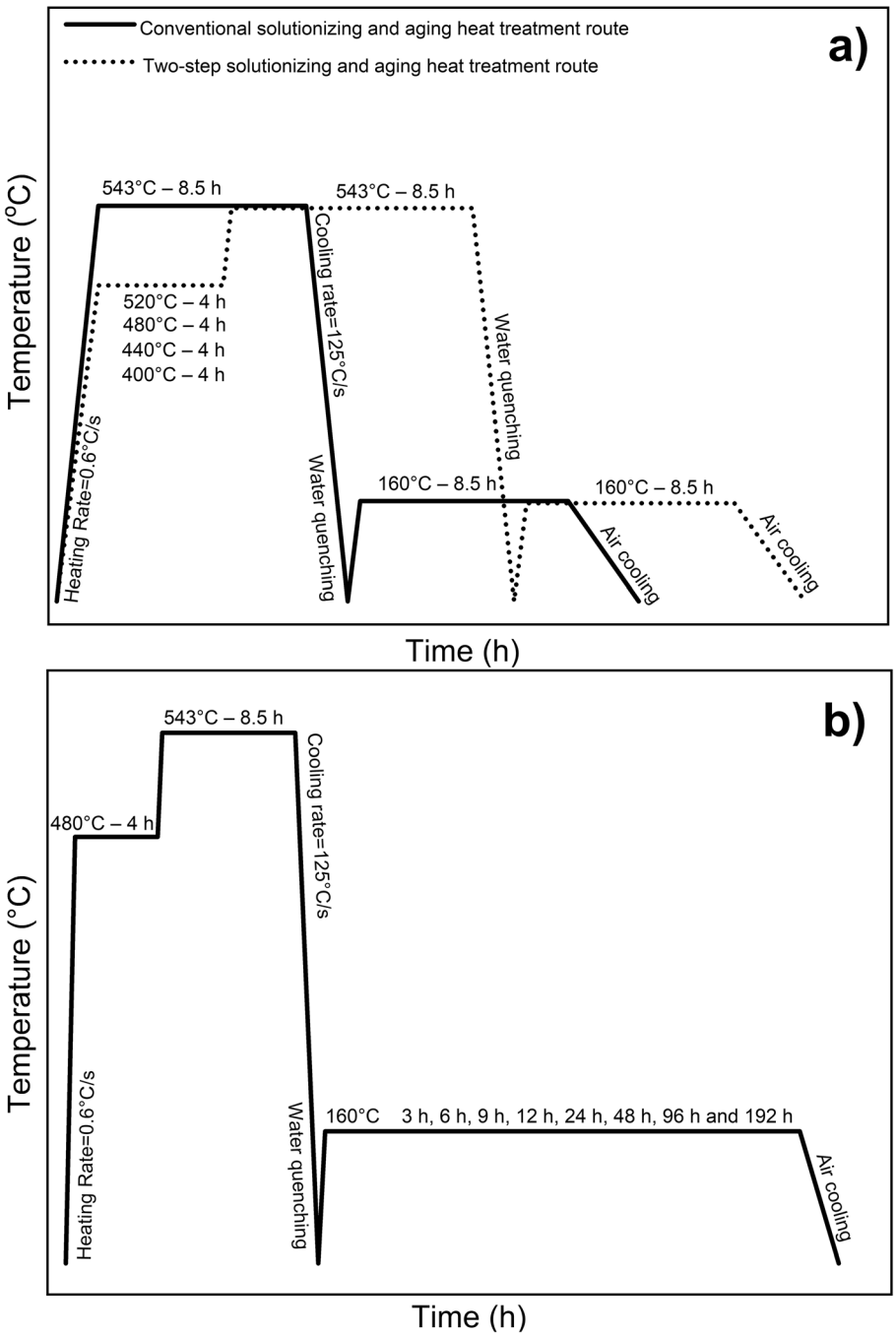

Figure 2. Schematic representation of heat treatment processes: (a) conventional solution and two-step solution treatments and (b) two-step solution treatments and different aging times.

known that the solution and aging treatments lead to the spheroidizing of Si particles in hypoeutectic Al–Si cast alloys (Figure 4b–f). Solution treatment temperatures significantly influence eutectic structure size, distribution, and morphology.[9–11,17] Si and other solute atoms solubility increase in α-Al phase with increasing solution temperatures up to the eutectic temperature. Moreover, higher solution temperatures lead to a more homogeneous distribution of spheroidized Si particles in the α-Al phase. The eutectic Si particles spheroidized and ripened with increasing solution temperatures and aging times (Figures 4b–f and 5a–h). It is noted that the eutectic Si particle size increases with increasing aging times (Figure 5a–h). Previous research demonstrated how the size and morphology of the initial eutectic Si particles influence the outcome during the solution treatment.[9–11,17,30] Lados et al.[10] reported that the eutectic Si particles transform, defined as fragmentation, globalization, and growth, respectively, during the solution treatment. They also

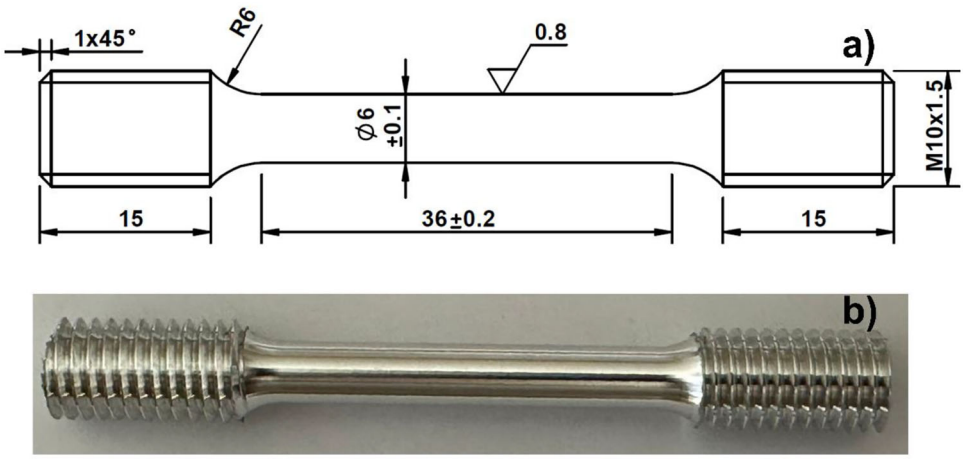

Figure 3. (a) Dimensions of the tensile sample and (b) the machined tensile sample.

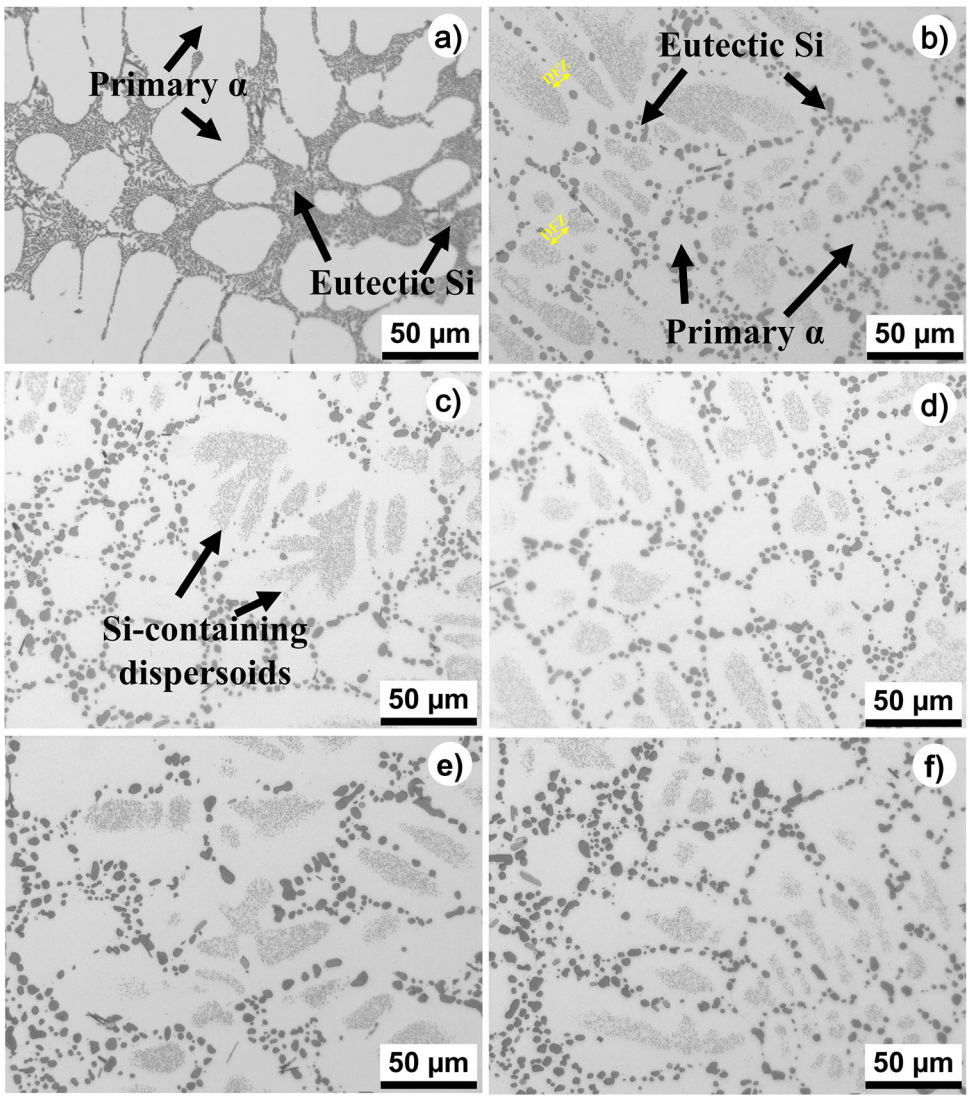

Figure 4. Optical microstructures of B357 alloy during solution treatment at different first-step solution temperatures. (a) as-cast, (b) conventional aging treatment, (c) 400 °C, (d) 440 °C, (e) 480 °C, (f) 520 °C. DFZ: dispersoid-free zones. Magnification: 500X.

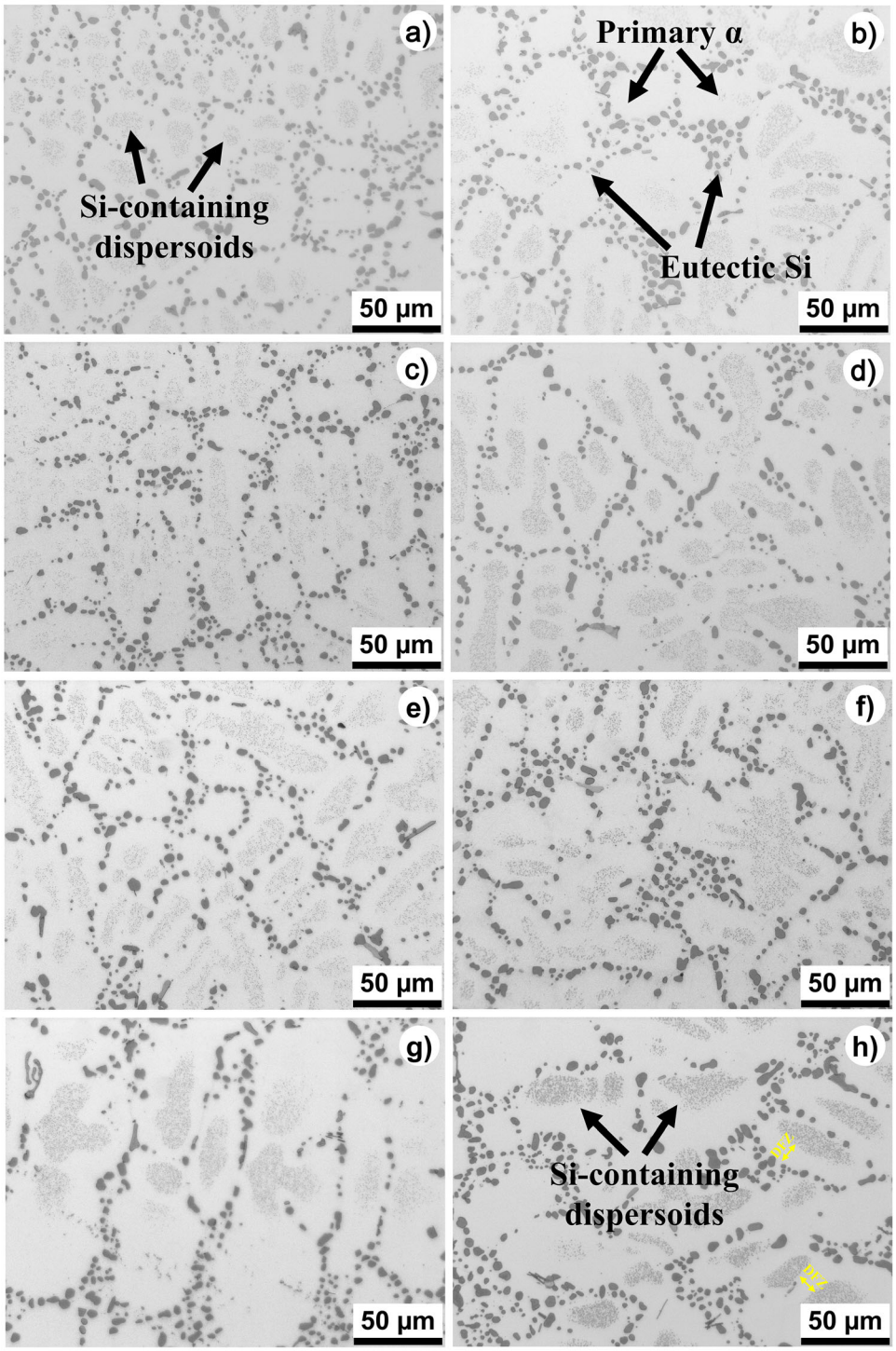

Figure 5. Optical microstructures of B357 alloy that two-step solutionized (480 °C–4 h→543 °C–8.5 h) and aged at 160 °C for different periods times: (a) 3 h, (b) 6 h, (c) 9 h, (d) 12 h, (e) 24 h, and (f) 48 h, (g) 96 h, and (h) 192 h. DFZ: dispersoid-free zones. Magnification: 500X.

reported that the eutectic Si particles became rounder and grew in less than 0.5 h in the modified alloy with Ce.

Quantitative analysis of eutectic Si particles according to solution temperatures and aging times are listed in Table 2. It shows that solution temperatures and aging times significantly affect the eutectic Si particles' size, area percentage, and count per area. The mean particle size of eutectic Si increased with increasing both solution temperatures and aging times (Table 2). Coarsening of eutectic Si particles during solution treatments and aging times has been widely reported for Al–Si–Mg cast

Table 2. Quantitative Analysis of Eutectic Si Particles According to Solution Temperatures and Aging Times

Samples	Area percent (%)	Mean particle size (μm)	Count per area (mm^{-2})
Conventional aging[¥]	8.5 ± 1	1.77 ± 0.51	19900 ± 2071
400 °C[§]	8.4 ± 1.1	1.53 ± 0.41	20950 ± 5185
440 °C[§]	8.6 ± 0.5	1.68 ± 0.37	16100 ± 1244
480 °C[§]	8.8 ± 1.3	1.99 ± 0.35	13500 ± 2521
520 °C[§]	10.4 ± 0.2	2.04 ± 0.46	13050 ± 2621
3 h*	7.4 ± 1.80	1.69 ± 0.4	21700 ± 4239
6 h*	8.1 ± 0.7	1.85 ± 0.32	16500 ± 4992
9 h*	8.8 ± 1.3	1.99 ± 0.35	13500 ± 2521
12 h*	9 ± 0.5	2.06 ± 0.36	13100 ± 4702
24 h*	9.3 ± 1	2.13 ± 0.33	12050 ± 3630
48 h*	9.6 ± 1	2.21 ± 0.41	11400 ± 2373
96 h*	9.9 ± 1.6	2.27 ± 0.43	11850 ± 4370
192 h*	10.4 ± 2.1	2.31 ± 0.42	11100 ± 3296

[¥]A conventional aging process is recommended according to the AMS 2771E standard[29]

[§]The temperatures are first-step solution temperatures. The second first-step solution was conducted at 543 °C for 4 h and 543 °C for 8.5 h. After a two-step solution, the samples were aged at 160 °C for 9 h

* The times are aging times. Two-step solution was conducted at 480 °C for 4 h and 543 °C for 8.5 h. The aging temperature is 160 °C

alloys.[8,10,11,13,15,19,21] The researchers reported that the particle size of eutectic Si increased with increasing solution temperatures and aging times.[10,19] Furthermore, solution temperatures and aging times increased the mean interparticle distance of eutectic Si particles (Figures 4b–f and 5a–h). It is well-known that an increase in the size of the eutectic Si particles leads to a corresponding increase in the average interparticle distance among these eutectic Si particles.[10,19,20] Additionally, the coarsening of eutectic Si particles reduced the number of particles per area. The number of particles per area decreases with increasing solution temperatures and aging times due to the coarsening of eutectic Si particles. Tiryakioglu[19] reported that during the solution treatment at 540 °C for up to 4h, the Si particles simultaneously grew and coarsened due to the supply of Si atoms diffusing out of the cores of dendrites. After the 4h solution treatment, the size of the eutectic Si particles follows the Lifshitz–Slyozov–Wagner (LSW) coarsening model.[19]

A small amount of Fe intermetallic (β-Al_5FeSi) compound was observed in this study due to the lower Fe concentration (0.086 wt.%) in the B357 alloy (Figure 6b). The researchers reported that Fe intermetallic compounds ($FeAl_3$, π-$Al_6Mg_3FeSi_6$, β-Al_5FeSi) were observed in the microstructure of A357 alloy.[5,12,31] It is well-known that the Fe intermetallic compounds are very detrimental to the mechanical properties of Al–Si cast alloy,[5,31] particularly fatigue life.[32]

Dark regions are observed in the middle region of primary-α dendrites in all aged samples. These regions are difficult to identify by examining optical microstructure images. Figure 6 shows the SEM microstructures of this region at high magnifications. These regions are identified as Si-containing dispersoids in the primary-α matrix according to EDX regional analyses (Figure 6b). It was observed that the dispersoids had rod and globular shape morphology (Figure 6c), and the average size of the dispersoids was measured below 500 nm. The formation of Si-containing dispersoids was also observed during the aging process of cast Al–Si–Mg alloys.[13,17,23,33] Chen et al.[23] and Lin[13,33] comprehensively studied the transformation mechanism of Si-containing dispersoids. The primary-α dendrites grow and absorb the Ti from the surrounding melt, initially having a higher Ti composition. In the as-cast hypoeutectic Al–Si–Mg alloy, eutectic Si dissolves by completely changing its morphology during the solution process; both Si and Ti atoms diffuse toward the dendrite arms. When the Ti composition exceeds the critical radius, nucleation of dispersoids occurs, leading to the formation of dispersoid-free zones (DFZ).[13,23,33] The width of the DFZ increases with increasing solution temperatures and aging times. Dispersoid zones in primary-α dendrites were also significantly reduced.[13,33] The area of Si-containing dispersoids decreases with increasing solution temperatures and aging times (Figures 4b–f and 5–h). In addition, the dispersoid regions are getting smaller in the middle of the primary-α dendrites with increasing solution temperatures and aging times (Figures 4b–f and 5a–h). Lin et al.[13] reported that the shape of dispersoids begins to change from ellipse and rod shape to spherical shape with increasing solution temperatures and aging times. On the other hand, increasing the solution temperature causes the growth of eutectic Si particles due to the high diffusion rate.[10,11,19,20,34] The authors reported the same phenomenon in their studies.[13,17,23,33] Lin et al.[13] reported that the presence of Si-containing dispersoids contributes up to 8-23 MPa to the strength of aged Al–Si–Mg alloy.

The characteristic aging steps of SSSS in Al–Si–Mg-based alloys proceed in a sequence consisting of the following stages: SSSS → GP zones → β' phase → β phase (Mg_2Si).[35] It is well-known that the supersaturation of Si and Mg solute atoms in primary-α Al leads to precipitation of a nano-scale strengthening Mg_2Si precipitates in the α-Al matrix during aging.[12] Precipitation of Mg_2Si in the primary-α matrix leads to distortion of the crystal lattice, inhibiting dislocation mobility during aging. This inhibited dislocation motion significantly increases the strength of the alloy.[10,11] Since Mg_2Si precipitates will form at the nano-scale, further TEM studies are required to confirm its presence.

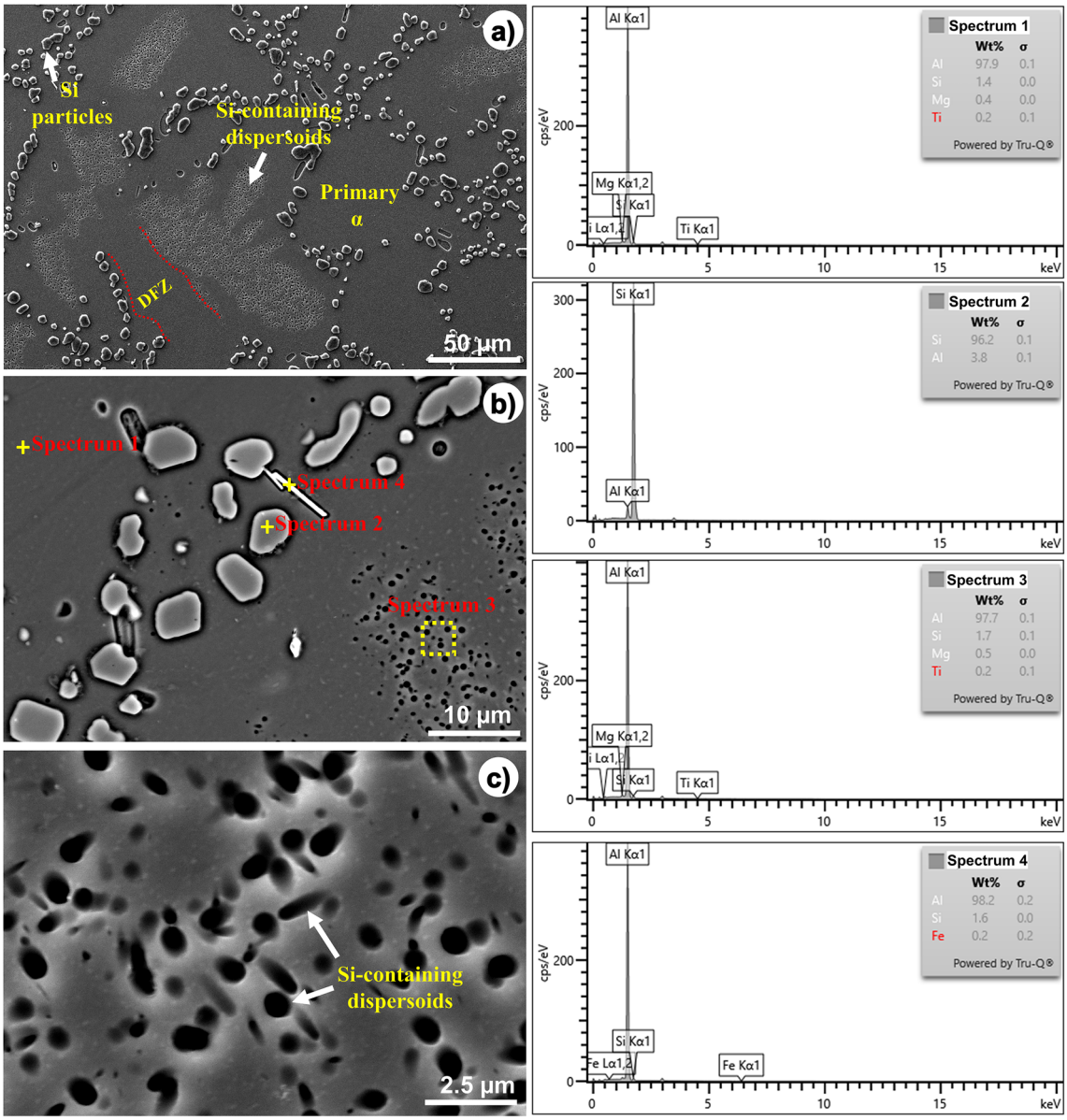

Figure 6. SEM microstructures and EDX analyses of B357 alloy; two-step solution was carried out at 480 °C for 4h and 543 °C for 8.5 h. The aging temperature is 160 °C for 9 h. (a) magnification: 1000X, (b) magnification: 5000X, (c) magnification: 20,000X.

Figure 7 illustrates XRD patterns of B357 samples according to first-step solution temperatures. Small Si and strong α-Al peaks were determined for all solution temperatures. It is compatible with the existing literature.[34,36,37] However, Mg_2Si precipitates could not be detected due to the low volume fraction. It should be noted that a phase detectable in XRD patterns has a volume fraction greater than 5%.[38] As mentioned above, a transmission electron microscopy study is needed to characterize the Mg_2Si precipitates.

DSC analyses were performed to evaluate how the two-step solution treatment affected the kinetics of Mg_2Si precipitation in the B357 alloy. Figure 8 shows the DSC curves of the B356 alloy subjected to solutionized at 543 °C for 8.5 h and a two-step solution treatment at 480 °C for 4h + 543 °C for 8.5 h, followed by artificial aging at 160 °C for 9 h. The curves were shifted vertically to improve visual observation along the y-axis. Two separate exothermic peaks can be identified for the two-step solution treatment at 214 °C and around 272 °C.

The higher peak temperatures (Tp) were found to be 222.7 and 277.2 °C for conventional aging treatment. In the two-step solution for B357 alloys, compared to the conventional aging treatment, there is an increase in the peak area and a decrease in the peak temperature (Tp) observed for β' (Mg_2Si) precipitates. A two-step solution treatment can be considered to increase the amount of β' precipitates in the B357 alloy for Mg2Si precipitate strengthening. The area

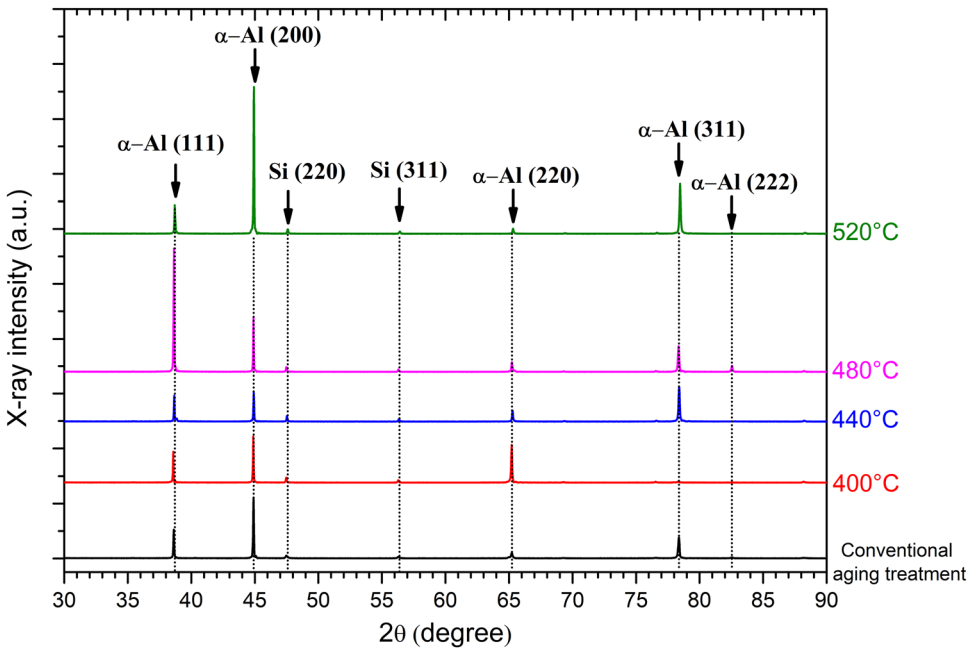

Figure 7. XRD pattern of B357 alloy according to first-step solution temperatures.

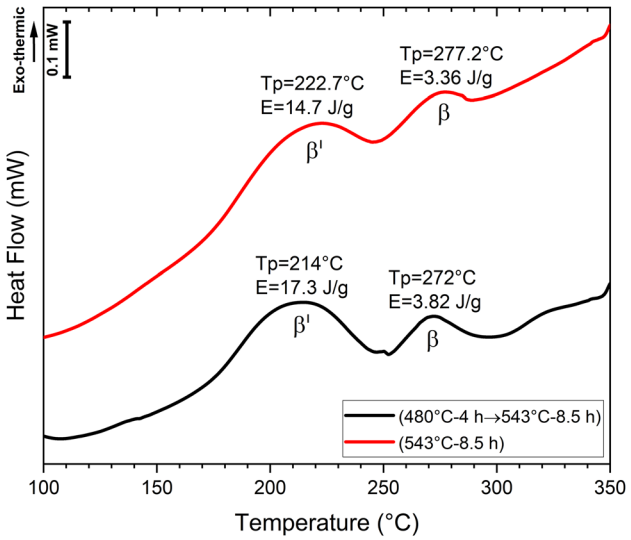

Figure 8. DSC curves of B357 alloy according to various solution treatments (Tp: temperature of peaks, E: dissolution enthalpy).

of the exothermic reaction (dissolution enthalpy) is approximately 17.3 and 14.7 J/g for the two-step solution and conventional aging treatments, respectively. The area of the reaction peaks represents the heat associated with the precipitation or dissolution of certain phases within Al alloys.[39] The energy released or absorbed is directly related to the volume fraction of precipitates. When the volume fraction of precipitates increases, the enthalpy of dissolution increases and the reaction temperature decreases. Thus, DSC analysis explains that two-step solution treatment can enhance the precipitation kinetics and the amount of Mg_2Si. The β' precipitates show an increasing peak area with a decreasing peak temperature (Tp) in two-step solution treatment. These results are consistent with the DSC analyses reported by Tan et al.[39] Higher peak areas and lower peak temperatures have been reported to favor increased precipitation transformation.[12,18,34]

Mechanical Properties

Mechanical properties of B357 alloy samples according to first-step solution temperatures and aging times are given in Table 3. Figure 9 illustrates the impact of first-step solution temperatures and aging times on mechanical properties. Compared to conventionally aged samples, the highest strength and good ductility were obtained in the two-step solutionized and aged sample (480 °C–4 h →543 °C–8.5 h → 160–9 h) (Table 3).

Increasing the first-step solution temperature from 400 to 480 °C significantly improved the mechanical properties (Table 3 and Figure 9a). In contrast, the mechanical properties decreased at the first-solution temperature of 520 °C. Two strengthening mechanisms can explain this situation. These are precipitation hardening and dispersion strengthening. Increasing the solution temperature causes more solute atoms to dissolve in the primary-α matrix, thus enhancing the formation of SSSS.[10,12,26,34,36] Increasing the degree of SSSS significantly improves strength and hardness.[5,10,16,20,27,36] On the other hand, increasing the first-step solution temperature to 520 °C leads to coarsening and coalescence of eutectic Si particles.[10,11] As mentioned above, researchers[10,11,19] reported that eutectic Si particles coarsen at higher solution temperatures, causing a decrease in mechanical properties. Moreover, uniformly

Table 3. Mechanical Properties of B357 Alloy Samples According to Solution Temperatures and Aging Times

First-step solution temperature and time	Second-step solution temperature and time	Aging times at 160 °C	Yield strength (MPa)	Ultimate tensile strength (UTS) (MPa)	Total elongation (TE) (%)	Hardness (HB 2.5/ 31.25 kgf)
As-cast			125.8 ± 4.5	213.7 ± 6.6	7.9 ±1.1	67 ± 1.5
–	543 °C–8.5 h	9 h	246.8 ± 17.4	331 ± 13.3	10.4 ± 1.4	108.6 ± 1.3
400 °C–4 h	543 °C–8.5 h		248.5 ± 7.7	327.9 ± 7	10.2 ± 1.8	103 ± 1.2
440 °C–4 h			248.6 ± 3.4	333 ± 3.2	10.5 ± 1.8	104 ± 1.1
480 °C–4 h			270.5 ± 9.9	345.7 ± 6	9.6 ± 1.2	108.2 ± 1.5
520 °C–4 h			255.5 ± 17.9	325 ± 14	6.3 ± 1.9	111.6 ± 1.3
480 °C–4 h	543 °C–8.5 h	3 h	171.9 ± 4.2	284.1 ± 4.3	11.6 ± 1	85 ± 1.3
		6 h	211.5 ± 4.7	308 ± 4.6	10.2 ± 1.5	93 ± 1.4
		9 h	270.5 ± 9.9	345.7 ± 6	9.6 ± 1.2	104 ± 2.5
		12 h	271.4 ± 5.3	350.4 ± 5	9.4 ± 1.5	108 ± 1.5
		24 h	301.5 ± 6	356.2 ± 6.5	7.2 ± 1.8	115 ± 1.1
		48 h	309.7 ± 4.8	366.1 ± 3.7	6 ± 1.5	120 ± 1
		96 h	307.3 ± 6.8	348.1 ± 3.7	4.9 ± 1.8	116 ± 1.5
		192 h	299.5 ± 4.4	338.3 ± 6.5	4.2 ± 1.0	114 ± 1

distributed and fine eutectic Si particles strengthen Al–Si–Mg casting alloys.[10,11] In this study, the Si particles were uniformly distributed in the matrix due to the Sr modification. However, higher solution temperatures lead to an increase in the size of the eutectic Si particles, leading to a decrease in the total elongation (Figure 9a).

As mentioned above, high solution temperature causes a decrease in the regions of Si-containing dispersoids in the primary-α matrix and increases the DFZ region (Figure 4). This decreased yield strength from 270.5 to 255.5 MPa and a total elongation from 9.6 to 6.3% in the first-step solution-treated sample processed at 520 °C (Table 3). It can be seen that 480 °C–4 h → 543 °C–8.5 h → 160–9 h sample provides the highest strength with ductility of 9.6% (Table 3 and Figure 8a). Due to its better mechanical properties, the first-step solution temperature was chosen as 480 °C for two-step solution treatments. Additionally, DSC analysis helps explain the precipitation reactions in the two-step solution treatments. The DSC analyses proved that the two-step solutionized (480 °C–4 h → 543 °C–8.5 h) B357 alloy exhibits more β' precipitates, as mentioned above (Figure 8). It is well-known that a direct relationship exists between increasing the volume fraction of precipitates and increases in strength and hardness (Table 3), as observed in two-step solution treatments.[9,27]

The relationship between mechanical properties and aging times in two-step solutionized (480 °C–4 h →543 °C–8.5 h) and aged samples is illustrated in Figure 9b. Yield strength, tensile strength, and hardness increased with increasing aging times in the two-step solutionized and aged B357 samples (Figure 9b and Table 3). However, the total elongation steadily decreases with increasing aging times (Figure 9b). It can be attributed to the aging kinetics of cast Al–Si–Mg alloys.[10,35] It is well-known that precipitation hardening causes a significant increase in strength and hardness, but total elongation decreases with

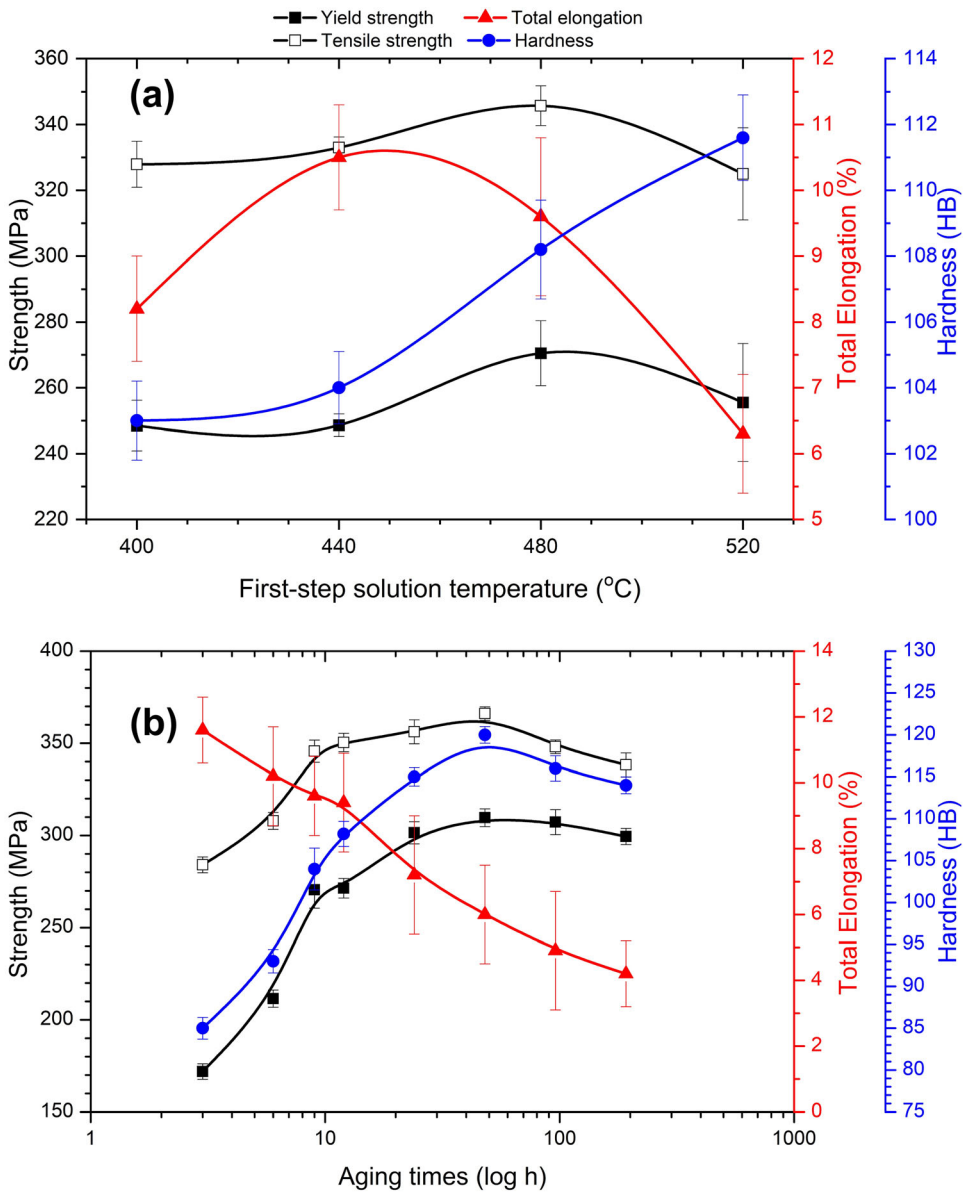

Figure 9. Mechanical properties of B357 alloy: (a) effect of solution temperatures (the temperatures are first-step solution temperatures. The second first-step solution was conducted at 543 °C for 4 h and 543 °C for 8.5 h. After a two-step solution, the samples were aged at 160 °C for 9 h), and (b) effect of aging times (the times are aging times. Two-step solution was conducted at 480 °C for 4 h and 543 °C for 8.5 h. The aging temperature is 160 °C).

the aging times.[6,8,10,20,24] The decrease in total elongation with increasing aging times can be attributed to the increase in the volume and the growth of the precipitates. This increased volume of the precipitates inhibits the movement of dislocations, making it more difficult for the material to deform plastically.[7,10–12,23,34,36,40] The study shows that B357 alloy exhibits 4.9% total elongation under overaged conditions (aging time: 96 h). Tirkayoglu and Alexopoulos[20] also reported that A357 alloy has a nominal minimum elongation to fracture of approximately 5% under overaged conditions. In addition, as mentioned above, the coarsening of the eutectic Si particles reduced the total elongation (Table 3). The peak strength and hardness were obtained at 48 h aging times in a two-step solutionized B357 alloy (Table 3 and Figure 9b). The yield and tensile strength were found to be decreased after 48 h aging times. The sample aged at 48 h exhibited the highest yield strength (309.7 MPa) and tensile strength (366.1 MPa) with 6% total elongation. Both yield and tensile strength decreased after 48 h (Table 3 and Figure 9b). It is attributed to the coarsening of Mg_2Si precipitates during aging, increased DFZ regions, and the decreased Si-containing dispersoid zones in the primary-α dendrites (Figure 5). Lin et al.[13] and Chen[23] reported that increasing the

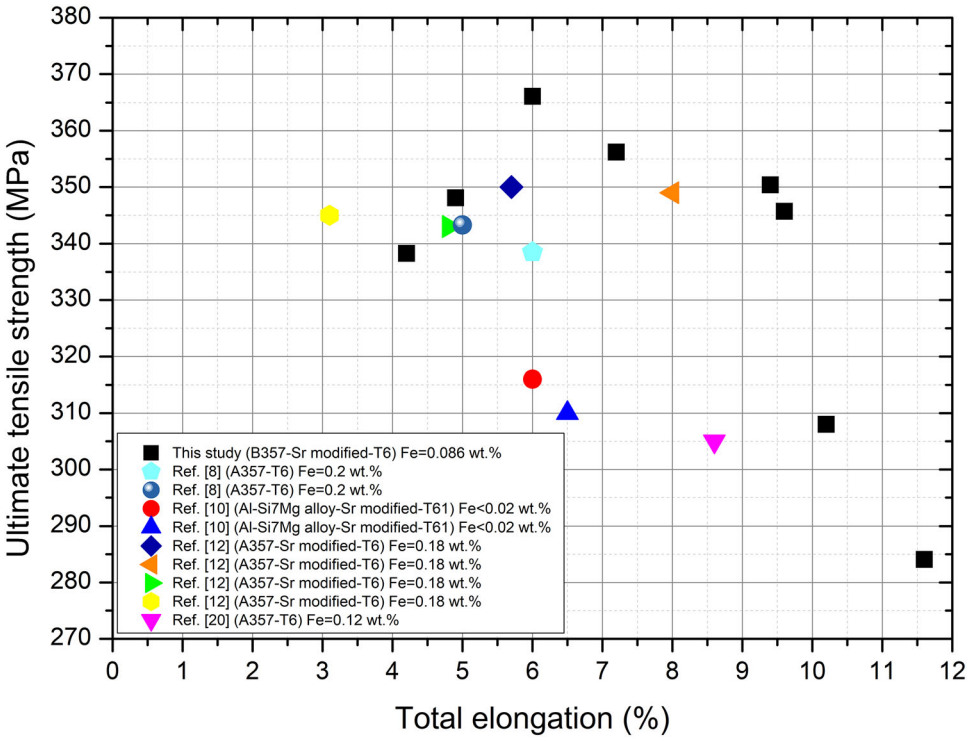

Figure 10. Comparison of ultimate tensile strength and total elongation of artificially aged current 357 alloys in this study with Al-Si alloys from previous studies.[8,10,12,20] Solution temperatures and times; 543 °C–8 h→ 154 °C–6 h and 543 °C–8 h→160 °C–7.5 h, cylindrical tensile bar with 0.5″ diameter in permanent mold casting,[8] 538 °C-10 naturally aged and 538 °C–10 h→155 °C–10 h, cylindrical tensile bar with 0.5″ diameter in cast iron mold,[10] 540 °C–6 h, 8 h, 10 h→175 °C–1 h to 10 h, 3.5 mm width and 2.2 mm thickness rectangular shape in Y-shaped iron molds,[12], 540 °C–22 h→155 °C–5 h to 20 h, continuously cast bars.[20]

Si-containing dispersoid zones improved the strength of the cast Al–Si–Mg alloy.

Figure 10 illustrates a comparison diagram for ultimate tensile strength (UTS) and total elongation (TE) in previous studies. It is noted that a much better combination of UTS and TE has been obtained in this study. Compared with previous studies, UTS and TE were improved with two-step solution treatment.[8–10] The highest UTS (366.1 MPa) was obtained in two-step solutionized samples at 480 °C for 4 h + 543 °C for 8.5 h and 160 °C for 48 h. The best combination of the UTS and TE (UTS = 350.4 MPa and TE = 9.4) have been obtained in two-step solutionized samples at 480 °C for 4 h + 543 °C for 8.5 h and aged 160 °C for 12 h. The improvement on the UTS and TE cannot depend only on the effect of two-step solution treatment, and they must also consider the casting method, Fe content, geometry, and dimensions of the tensile bar.

Fracture Surface Evaluation

The fracture surfaces of two-step solutionized and aged B357 alloy are shown in Figure 11. The colossal dimple depressions were evidence of ductile fracture at the fracture surface (Figure 11a). Significant ductile fracture regions were observed in the two-step solutionized and aged A357 alloy (Figure 11b and c). Ductile dimples were observed mainly in primary-α matrix regions (Figure 11c white arrows). Decohesion regions of Si particles from the surrounding primary-α matrix structure were observed in all samples (Figure 11c yellow arrows). Brittle fractured Si particles were also observed on the fracture surfaces (Figure 11c black arrows). The findings were consistent with previous research.[20]

Conclusions

This study investigated the effect of two-step solution treatments and aging times on the microstructures and mechanical properties of B357 alloy. The following conclusions were drawn from this study:

(1) The two-step solution treatment significantly increases the ultimate tensile strength from 284.1 to 366.1 MPa in B357 alloy.
(2) It was observed that different aging treatment conditions resulted in similar microstructures;

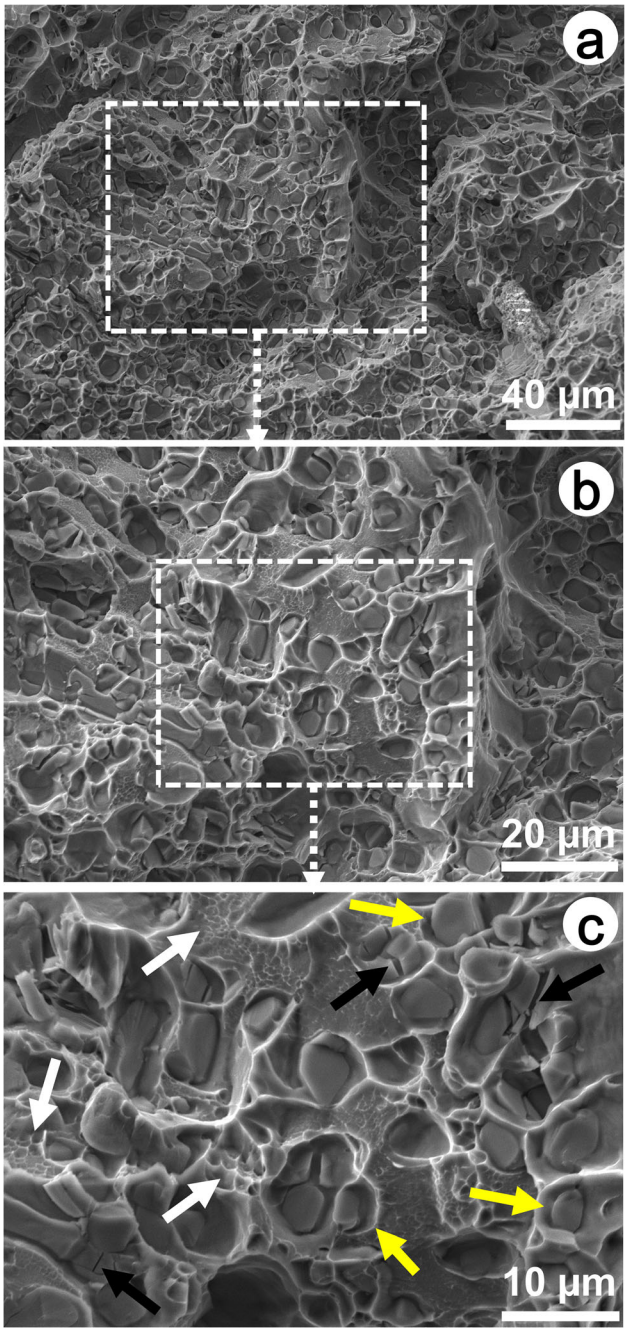

Figure 11. Fracture surfaces of two-step solutionized and aged B357 alloy (Two-step solution was conducted at 480 °C for 4h and 543 °C for 8.5 h. Aging temperature is 160 °C for 9 h). (a) magnification = 100X, (b) magnification = 2000X, and (c) magnification = 4000X. Black arrows show the brittle fracture in Si particles; white arrows show the fracture of ductile dimples, and yellow arrows show the decohesion between Si particles and matrix.

minor changes were attributed to the coarsening of Si particles. Eutectic Si particles spheroidized and ripened with increasing solution temperatures and aging times.

(3) Si-containing dispersoids and dispersoid-free zones (DFZ) were also observed in the primary-α matrix. The width of the DFZ increases with increasing solution temperatures and aging times. However, dispersoid zones in primary-α dendrites were also significantly reduced.

(4) DSC analyses showed that two-step solution treatment increased the amount of β' precipitates in the B357 alloy available for Mg_2Si precipitate strengthening.

(5) Compared with conventionally aged samples, the best combination of strength and ductility were obtained in the sample subjected into two-step solutionizing and aging (480 °C–4 h →543 °C–8.5 h → 160–9 h). The sample aged at 48 h exhibited the highest yield strength (309.7 MPa) and tensile strength (366.1 MPa) with 6% total elongation.

(6) Ductile fracture mode was the dominant fracture mode in all aged B357 alloy samples. Brittle fractured Si particles were observed in the fracture surfaces.

Acknowledgements

The authors would like to thank Altun Dokum A.Ş, Konya/Turkiye, for providing B357 alloy tensile bars and machining of the bars.

Funding

Open access funding provided by the Scientific and Technological Research Council of Türkiye (TÜBITAK).

Author Contributions

Neset Akar contributed to experimental studies (casting and heat treatments), investigation, creating figures, and writing. Omer Sahin contributed to experimental studies (mechanical tests and microstructural characterization studies), investigation, creating figures, and writing. Volkan Kilicli contributed to conceptualization, creating figures, writing, and editing.

Data Availability

The raw data cannot be shared at this time as the data are also part of an ongoing study.

Conflict of interest Authors declare they have no conflict of interest.

REFERENCES

1. I. Polmear, D. StJohn, J.-F. Nie, M. Qian, *Light Alloys: Metallurgy of the Light Metals* (Butterworth-Heinemann, 2017), pp.265–286
2. A.A. Luo, A.K. Sachdev, D. Apelian, Alloy development and process innovations for light metals casting. J. Mater. Process. Technol. (2022). https://doi.org/10.1016/j.jmatprotec.2022.117606
3. S.K. Chaudhury, D. Apelian, Effects of Mg and Cu content on quench sensitivity of Al-Si-Mg alloy. Int. J. Met. (2016). https://doi.org/10.1007/s40962-016-0020-z
4. H.R. Ammar, A.M. Samuel, F.H. Samuel, H.W. Doty, The concept of quality index and its application for Al–Si cast alloys. Int. J. Met. (2021). https://doi.org/10.1007/s40962-020-00556-6
5. E.A. Elsharkawi, M.F. Ibrahim, A.M. Samuel, H.W. Doty, F.H. Samuel, Understanding the effect of be addition on the microstructure and tensile properties of Al–Si–Mg cast alloys. Int. J. Met. (2021). https://doi.org/10.1007/s40962-021-00715-3
6. M.F. Ibrahim, A.M. Samuel, H.W. Doty, F.H. Samuel, Effect of aging conditions on precipitation hardening in Al–Si–Mg and Al–Si–Cu–Mg alloys. Int. J. Met. (2016). https://doi.org/10.1007/s40962-016-0057-z
7. U. Kutsal, Y. Arslan, O. Ozaydin, Y. Akyildiz, A. Yigit Kaya, O. Ertugrul, Heat treatment simulation of aluminum alloy wheels and ınvestigation of process steps. Int. J. Met. (2023). https://doi.org/10.1007/s40962-023-01132-4
8. O. Es-Said, D. Lee, W. Pfost, D. Thompson, M. Patterson, J. Foyos, R. Marloth, Alternative heat treatments for A357-T6 aluminum alloy. Eng. Fail. Anal. (2002). https://doi.org/10.1016/S1350-6307(00)00034-0
9. Y. Han, A.M. Samuel, H.W. Doty, S. Valtierra, F.H. Samuel, Optimizing the tensile properties of Al–Si–Cu–Mg 319-type alloys: role of solution heat treatment. Mater. Des. (2014). https://doi.org/10.1016/j.matdes.2014.01.060
10. D.A. Lados, D. Apelian, L. Wang, Solution treatment effects on microstructure and mechanical properties of Al-(1 to 13 pct)Si-Mg cast alloys. Metall. Mater. Trans. B (2011). https://doi.org/10.1007/s11663-010-9437-6
11. S. Shivkumar, S. Ricci, C. Keller, D. Apelian, Effect of solution treatment parameters on tensile properties of cast aluminum alloys. J. Heat. Treat. (1990). https://doi.org/10.1007/BF02833067
12. G. Asghar, L. Peng, P. Fu, L. Yuan, Y. Liu, Role of Mg_2Si precipitates size in determining the ductility of A357 cast alloy. Mater. Des. (2020). https://doi.org/10.1016/j.matdes.2019.108280
13. Y.C. Lin, S.-C. Luo, J. Huang, L.-X. Yin, X.-Y. Jiang, Effects of solution treatment on microstructures and micro-hardness of a Sr-modified Al–Si–Mg alloy. Mater. Sci. Eng. A (2018). https://doi.org/10.1016/j.msea.2018.04.049
14. V. Raveendranath, V.R. Aravind Senan, K. Venkateswarlu, K.V. Shankar, Solutionizing temperature effect on the dry sliding wear performance of Al-7Si-0.3Mg-3Ni hypoeutectic alloy. SILICON (2023). https://doi.org/10.1007/s12633-023-02339-0
15. L. Tonelli, E. Liverani, A. Morri, L. Ceschini, Role of direct aging and solution treatment on hardness, microstructure and residual stress of the A357 (AlSi7Mg0.6) alloy produced by powder bed fusion. Metall. Mater. Trans. B (2021). https://doi.org/10.1007/s11663-021-02179-6
16. K.T. Kashyap, S. Murali, K.S. Raman, K.S.S. Murthy, Casting and heat treatment variables of Al-7Si-Mg alloy. Mater. Sci. Technol. (1993). https://doi.org/10.1179/mst.1993.9.3.189
17. D. Qian, K. Lan, Y. Yang, The Effect of solution temperature on microstructure evolution and mechanical properties of a low-silicon cast aluminum alloy containing Mn. Int. J. Met. (2023). https://doi.org/10.1007/s40962-023-01138-y
18. M. Faccoli, D. Dioni, S. Cecchel, G. Cornacchia, A. Panvini, Optimization of heat treatment of gravity cast Sr-modified B356 aluminum alloy. Trans. Nonferrous Met. Soc. China (2017). https://doi.org/10.1016/s1003-6326(17)60192-4
19. M. Tiryakioğlu, Si particle size and aspect ratio distributions in an Al-7%Si-0.6%Mg alloy during solution treatment. Mater. Sci. Eng. A (2008). https://doi.org/10.1016/j.msea.2007.03.044
20. M. Tiryakioğlu, N.D. Alexopoulos, The effect of artificial aging on tensile work hardening characteristics of a cast Al-7 Pct Si-0.55 Pct Mg (A357) alloy. Metall. Mater. Trans. A (2008). https://doi.org/10.1007/s11661-008-9611-5
21. Y. Harada, S. Tamura, S. Kumai, Effects of high-temperature solutionizing on microstructure and tear toughness of A356 cast aluminum alloy. Mater. Trans. (2011). https://doi.org/10.2320/matertrans.L-MZ201105
22. A.M.A. Mohamed, F.H. Samuel, S. Al Kahtani, Influence of Mg and solution heat treatment on the occurrence of incipient melting in Al–Si–Cu–Mg cast alloys. Mater. Sci. Eng. A (2012). https://doi.org/10.1016/j.msea.2012.02.032

23. R. Chen, Q. Xu, Z. Jia, B. Liu, Precipitation behavior and hardening effects of Si-containing dispersoids in Al-7Si-Mg alloy during solution treatment. Mater. Des. (2016). https://doi.org/10.1016/j.matdes.2015.11.069
24. R.X. Li, R.D. Li, Y.H. Zhao, L.Z. He, C.X. Li, H.R. Guan, Z.Q. Hu, Age-hardening behavior of cast Al–Si base alloy. Mater. Lett. (2004). https://doi.org/10.1016/j.matlet.2003.12.027
25. P. Ouellet, F.H. Samuel, Effect of Mg on the ageing behaviour of Al–Si–Cu 319 type aluminium casting alloys. J. Mater. Sci. (1999). https://doi.org/10.1023/A:1004645928886
26. J. Pezda, Optimization of heat treatment parameters of AlSi7Mg alloy. Materials (2022). https://doi.org/10.3390/ma15031163
27. S. Toschi, Optimization of A354 Al–Si–Cu–Mg alloy heat treatment: effect on microstructure, hardness, and tensile properties of peak aged and overaged alloy. Metals (2018). https://doi.org/10.3390/met8110961
28. A. Samuel, J. Gauthier, F. Samuel, Microstructural aspects of the dissolution and melting of Al_2Cu phase in Al–Si alloys during solution heat treatment. Metall. Mater. Trans. A (1996). https://doi.org/10.1007/BF02651928
29. AMS 2771E-2013, Heat Treatment of Aluminum Alloy Castings (SAE International, 2013). https://webstore.ansi.org/standards/sae/saeamss2771e2013ams2771e. Accessed 4 Jan 2024
30. A.M. Samuel, M.H. Abdelaziz, H.W. Doty, F.H. Samuel, Metallurgical parameters controlling fragmentation and Spheroidization processes of eutectic Si particles in Al–Si cast alloys. Int. J. Met. (2021). https://doi.org/10.1007/s40962-021-00702-8
31. E.A. Elsharkawi, M.H. Abdelaziz, H.W. Doty, S. Valtierra, F.H. Samuel, Effect of β-Al_5FeSi and π-$Al_8Mg_3FeSi_6$ phases on the impact toughness and fractography of Al–Si–Mg-based alloys. Int. J. Met. (2017). https://doi.org/10.1007/s40962-017-0153-8
32. Q.G. Wang, D. Apelian, D.A. Lados, Fatigue behavior of A356/357 aluminum cast alloys Part II—effect of microstructural constituents. J. Light. Met. (2001). https://doi.org/10.1016/S1471-5317(00)00009-2
33. Y.C. Lin, S.-C. Luo, L.-X. Yin, J. Huang, Microstructural evolution and high temperature flow behaviors of a homogenized Sr-modified Al–Si–Mg alloy. J. Alloys Compd. (2018). https://doi.org/10.1016/j.jallcom.2017.12.278
34. Y. Birol, Effect of solution heat treatment on the age hardening capacity of dendritic and globular AlSi7Mg0.6 alloys. Int. J. Mater. Res. (2010). https://doi.org/10.3139/146.110293
35. M. Vlach, J. Čížek, B. Smola, O. Melikhova, M. Vlček, V. Kodetová, H. Kudrnová, P. Hruška, Heat treatment and age hardening of Al–Si–Mg–Mn commercial alloy with addition of Sc and Zr. Mater Charact (2017). https://doi.org/10.1016/j.matchar.2017.04.017
36. Y. Birol, Response to artificial ageing of dendritic and globular Al-7Si-Mg alloys. J. Alloys Compd. (2009). https://doi.org/10.1016/j.jallcom.2009.05.043
37. K.V. Yang, P. Rometsch, C.H.J. Davies, A. Huang, X. Wu, Effect of heat treatment on the microstructure and anisotropy in mechanical properties of A357 alloy produced by selective laser melting. Mater. Des. (2018). https://doi.org/10.1016/j.matdes.2018.05.026
38. B.D. Cullity, S.R. Scott, *Elements of X-Ray Diffraction* (Prentice-Hall, NJ, 2001), pp.347–361
39. Y.-H. Tan, S.-L. Lee, Y.-L. Lin, Effects of Be and Fe additions on the microstructure and mechanical properties of A357.0 alloys. Metall. Mater. Trans. A (1995). https://doi.org/10.1007/BF02670615
40. K. Du, Q. Zhu, D. Li, F. Zhang, Study of formation mechanism of incipient melting in thixo-cast Al–Si–Cu–Mg alloys. Mater Charact (2015). https://doi.org/10.1016/j.matchar.2015.05.035